

Article

# Influence of NaCl Freeze Thaw Cycles and Cyclic Loading on the Mechanical Performance and Permeability of Sulphoaluminate Cement Reactive Powder Concrete

Xinghua Hong <sup>1,2</sup> , Hui Wang <sup>3,\*</sup> and Feiting Shi <sup>4</sup>

<sup>1</sup> College of Textiles (International Silk Institute), Key Laboratory of Advanced Textile Materials and Manufacturing Technology, Ministry of Education, Zhejiang Sci-Tech University, Hangzhou 310018, Zhejiang, China; xinghuahong@zstu.edu.cn

<sup>2</sup> Tongxiang Research Institute, Zhejiang Sci-Tech University, Tongxiang 314599, Zhejiang, China

<sup>3</sup> State Key Laboratory of Materials-Oriented Chemical Engineering, Nanjing 210000, Jiangsu, China

<sup>4</sup> Civil Engineering Department, Yancheng Institute of Technology, Yancheng 224051, Jiangsu, China; feitingshi@aliyun.com

\* Correspondence: huiwang123@aliyun.com

Received: 25 November 2020; Accepted: 11 December 2020; Published: 16 December 2020



**Abstract:** This paper aimed to investigate the coupling effects of NaCl freeze–thaw cycles and cyclic loading on the mechanical performance and permeability of sulphoaluminate cement reactive powder concrete (RPC). Firstly, the compressive and flexural strengths of sulphoaluminate cement RPC were investigated. Then, the chloride ion permeability, mechanical strengths (compressive and flexural strengths) and mass loss were determined. Results indicated that the increased steel fibers content and curing age played positive roles in the mechanical strengths. The threshold values of steel fibers and curing age were 3.0% and 14 days. Sulphoaluminate cement RPC with early curing age (5 h) showed relatively high mechanical strengths: flexural strength (8.69~17.51 MPa), and compressive strength (34.1~38.5 MPa). The mass loss, the chloride migration coefficient, and the compressive strength loss increased linearly with NaCl freeze–thaw cycles. Meanwhile, the flexural strength loss increased with the exponential function. The relative dynamic modulus of elasticity of specimens decreased linearly with the increased freeze–thaw cycles. Finally, it was observed from this paper, cyclic loading demonstrated negative roles on the mechanical strengths and resistance to chloride penetration.

**Keywords:** sulphoaluminate cement; reactive powder concrete; mechanical strengths; chloride migration coefficient; NaCl freeze–thaw cycles

## 1. Introduction

Under the complicated external impacts, such as vehicle overload, fatigue loading, freeze–thaw cycle, seawater erosion, freeze–thaw cycle and seawater erosion, bridges and highways usually suffer cracks and spalling. For timely and normal operation of roads and bridges, rapid hardening concrete should be fabricated. Based on concrete with high strength, excellent durability, rapid hardening, and construction feasibility, it is necessary to develop rapid hardening concrete with high mechanical strength and durability.

Reactive powder concrete (RPC) is called ultra-high-performance concrete, which was first invented in the 1990s by the Bouygues Company on the basis of maximum density. This kind of concrete is composed of cement, many mineral admixtures, and quartz sand. Furthermore, it does not contain any coarse aggregate. Characterized by optimal particle size distribution of quartz sand

and high active mineral admixtures, RPC exhibits excellent mechanical and durable properties. Rajasekar et al. [1–3] reported that the addition of micro steel fibers was sufficient to improve the compressive and flexural strengths to 130 and 44.21 MPa, respectively. Xu et al. [4] found that the addition of waste steel fibers could improve the mechanical performance of RPC and were adequate substitutes for copper-coated steel fibers. Wang et al. [5] pointed out that RPC with carbon nanofibers shows ultra-high-strength, strain self-sensing performance and deicing properties. Micro steel/stainless fiber is an effective way to help RPC become conductive, self-sensing, and more ductile material [6,7]. Although, the mechanical performances of RPC were investigated widely. The researchers mainly aimed to focus on the Portland cement based RPC. At present, the research on sulphoaluminate cement fast hardening RPC is still blank.

As reported by Nematollahzade [8], the Portland cement based materials should be cured for more than three days before using. Sulphoaluminate cement, as a kind of quick hardening cement, has been applied to the repair of roads and bridges. As shown in Feng's paper [9], for the 3 h cured sulphoaluminate cement mortar with micro-fine steel fibers, it displayed a maximum compressive strength of 19 MPa and flexural strength of 5.3 MPa. Prior researches [10–12] pointed out that the mechanical strength of Portland cement based materials at initial curing age (3 h~3 days) was much lower than that of sulphoaluminate cement based materials, while at a long curing age, the mechanical strength of Portland cement based materials showed higher strength than sulphoaluminate cement based materials.

Although a significant number of studies were carried out on sulphoaluminate cement-based materials, little attention was paid to the research of combining the advantages of sulphoaluminate cement and RPC.

Concrete construction buildings usually suffered from corrosive actions when exposed to the marine environment. The corrosive effects of marine concrete structures like seawater freeze–thaw cycles and chloride penetration usually lead to the corrosion of steel bars or steel fibers in concrete; hence, the durability and reliability of civil structures built by concrete descended [13,14]. By now, the influence of NaCl freeze–thaw cycles and chloride penetration on the performance degradation has been reported in many studies [15–17]. However, few researchers considered the coupling effects of NaCl freeze–thaw cycles and cyclic loading on the mechanical performance and permeability of sulphoaluminate cement RPC.

In this paper, the sulphoaluminate cement RPC was manufactured and the mechanical strengths (compressive strength and flexural strength) were cured in standard environment for 5 h, 1 day, 14 days and 28 days. The mass and mechanical strengths' losses were determined when the specimens were exposed to the environment of 50, 100, 150, 200, 250 and 300 NaCl freeze–thaw cycles. Additionally, the relative dynamic elastic modulus (RDME) and chloride migration coefficient (CMC) were tested during the NaCl freeze–thaw cycles.

## 2. Experimental Schemes

### 2.1. Raw Materials and Mixing Proportion

Copper-coated steel fibers with a density of 7.93 g/cm<sup>3</sup>, length of 12–14 mm, diameter of 0.18–0.23 mm and aspect ratio of 60 supplied by Anshan COBIT Co., Ltd., Anshan, China, were used in this study. The tensile strength of this copper coated steel fiber was 3100 MPa. RC.SAC fast hard sulphoaluminate cement produced by Tangshan polar bear building materials Co., Ltd., Tangshan, China, with a strength grade of 42.5 MPa was applied in this research. Silica fume (SF) and granulated blast furnace slag powder (GGBS) were used as other cementitious materials. The silica fume possesses a specific surface area of 15 m<sup>2</sup>/g and more than 98% SiO<sub>2</sub>. The density of SF is 2.2 g/cm<sup>3</sup>. The GGBS applied in this study shows a density of 2.9 g/cm<sup>3</sup>, a specific surface area of 436 m<sup>2</sup>/g and a loss on ignition of 2.3%. The performance index of cement, SF and GGBS meets the requirements of GB175-2007, GB/T21236-2007 and GB/T-18046-2008 [18–20], respectively. Quartz sand with three kinds of particle

sizes of 1~0.71, 0.59~0.35 and 0.15~0.297 mm, with mass ratios of 1:1.5:0.2, were used as aggregate. Moreover, they were composed of 99.6% SiO<sub>2</sub>, 0.02% Fe<sub>2</sub>O<sub>3</sub> and other ingredients. The binder sand ratio of RPC in this study was 1.25. The polycarboxylate-based, high-range water-reducing agent with a 40% water-reducing rate was applied in adjusting the fluidity of fresh RPC paste. The SF, GGBS and Polycarboxylate-based, high-range water-reducing agents were produced by Shenteng Co., Ltd., Lingshou, China. Tables 1 and 2 show the particle size distribution and chemical composition of cementitious materials. Li<sub>2</sub>SO<sub>4</sub>, tartaric acid, polyether produced by Yingshan, Co., Ltd., Shanghai, China, were used as early strength agent, retarder and defoamer in this study.

**Table 1.** Particle size distribution of the raw materials/%.

Particle Size/ $\mu\text{m}$							
	0.3	0.6	1	4	8	64	360
Types							
Cement	0	0.33	2.66	15.01	28.77	93.59	100
Slag power	0.025	0.1	3.51	19.63	35.01	97.9	100
Silica fume	31.2	58.3	82.3	100	100	100	100

**Table 2.** Chemical composition of the cementitious materials.

Types	SiO <sub>2</sub>	Al <sub>2</sub> O <sub>3</sub>	Fe <sub>2</sub> O <sub>3</sub>	MgO	CaO	SO <sub>3</sub>	Ti <sub>2</sub> O
Cement	13.95	22.46	2.67	2.92	39.39	14.34	1.66
Slag power	34.06	14.74	0.23	9.73	35.93	0.23	3.51
Silica fume	90	0.2	0.6	0.2	0.4	0	7.4

The copper-coated steel fibers with dosages of 0%, 1.0%, 1.0%, 2.0%, 3.0%, and 4.0% by the RPC volume were added to the mixture to determine the mechanical strengths. The fabricated specimens were used to study their mechanical strengths. In addition, specimens with 3.0% steel fibers were further used to perform mechanical strength loss (compressive strength loss and flexural strength loss), the RDME and CMC during freeze–thaw cycles.

To manufacture sulphoaluminate cement RPC, sulphoaluminate cement, silica fume, slag powder, quartz sand, and all powder admixture were mixed first in UJZ-15 mortar mixer for 0.5 min, and then steel fibers were added and mixed for another 2 min. After this mixing, the water-reducing agent was mixed with water and stirred in the mixture for the last 5.5 min. Specimens with a size of 40 × 40 × 160 mm<sup>3</sup> were applied to determine the mechanical strengths after cured in a standard curing environment (temperature of 20 ± 2 °C and relative humidity of above 95%) for 5 h, 1 day, 14 days and 28 days respectively.

Specimens with a size of 40 × 40 × 160 mm<sup>3</sup> and  $\Phi$ 100 × 50 mm<sup>2</sup> were used for the mechanical strengths loss and the measurement of CMC, respectively, after different freeze–thaw cycles. Specimens with a size of 100 × 100 × 400 mm<sup>3</sup> were used for the experiment of mass loss and relative dynamic modulus of elasticity during freeze–thaw cycles. In this part, all specimens were cured in standard curing environment for 24 days. After curing for 24 days, all specimens were immersed in 3% NaCl solution for 4 days before freeze–thaw cycles.

## 2.2. Measurement Methods

WDW-200E with maximum applied load of 200 kN was provided for the mechanical strength and toughness test. Compressive and flexural strengths were conducted according to Chinese standard GB/T17671-1999 [21]. The freeze–thaw test was carried out following Chinese Standard GB/T 50082-2009 [22]. Every specimen was placed in a rubber tube in the rapid freeze–thaw testing machine. The rubber tubes were filled with 3.0% NaCl solution and were covered by plastic sheets to avoid water evaporation. After different freeze–thaw cycles, the degradation state of RPC was evaluated by the

evolution of mass loss and RDME. Additionally, the variations of mechanical strengths loss and CMC were tested during NaCl freeze–thaw cycles. Before NaCl freeze–thaw cycles, some selected specimens were treated with 100 cycles of load–unload (each cycle lasted 1 s). The cyclic load level ranged from 0% to 30% of the axial flexural strength or splitting tensile strength of cylinder ( $\Phi 100 \times 50 \text{ mm}^2$ ). The cyclic loading applied in specimens for the CMC measurement is shown in Figure 1. The CMC experiment was conducted as follows: Firstly, the water on the surface of cylinders ( $\Phi 100 \times 50 \text{ mm}^2$ ) was wiped out and then the specimens were immersed in the deionized water in the concrete intelligent vacuum water Saturator vacuum desiccator for the water saturation treatment. After that, the sides of the treated specimen were sealed by silica gel. Finally, the specimens were settled in the chloride ion diffusion coefficient tester. The details for this experiment can refer to the Chinese Standard GB/T 50082-2009 [22].

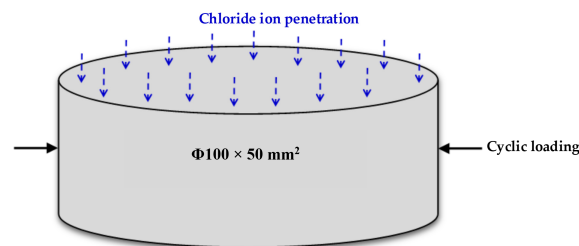


**Figure 1.** Cyclic loading applied in specimens for the chloride migration coefficient (CMC) measurement.

### 3. Results and Discussion

#### 3.1. Mechanical Strength

Figure 2 shows the flexural and compressive strengths of sulphoaluminate RPC. It can be observed that the flexural and compressive strengths of sulphoaluminate cement RPC increased with the increasing dosage of steel fibers (0~4%) and the curing time. When the dosage of steel fibers ranged from 3% to 4%, the mechanical strengths rarely changed. This was attributed to the fact that the steel fiber reinforced network was relatively complete leading to the stability of mechanical properties. Additionally, more steel fibers agglomerated if the addition of fiber content was 4% than that of 3%, leading to limiting the mechanical strength of sulphoaluminate cement RPC. As shown in Figure 2, the flexural strength of sulphoaluminate cement RPC ranged from 8.69 to 17.51 MPa when cured for 5 h. Meanwhile, at the same curing age, the compressive strength of sulphoaluminate cement RPC ranged from 34.1 to 38.5 MPa. The maximum growth rate of flexural strength was 101.5% and the maximum growth rate of compressive strength was 12.9%. This was attributed to the fact that at an early curing age (5 h), the compressive strength mainly depends on the strength of the RPC matrix [23,24]. Consequently, the flexural strength was dominated by steel fibers. Therefore, at early curing ages, the addition of steel fibers had more pronounced influence on the flexural strength than that of compressive strength. However, when the curing ages were 1 day, 14 days and 28 days, the maximum growth rates of flexural strength were 71.2%, 121.3% and 135.2%. Simultaneously, the maximum growth rates of the compressive strength were 51.2%, 71.4% and 67.5%. This was attributed to the fact that the hydration degree tended to be stable with the increasing curing age [16]. Therefore, steel fibers demonstrated more active roles on the mechanical strengths.

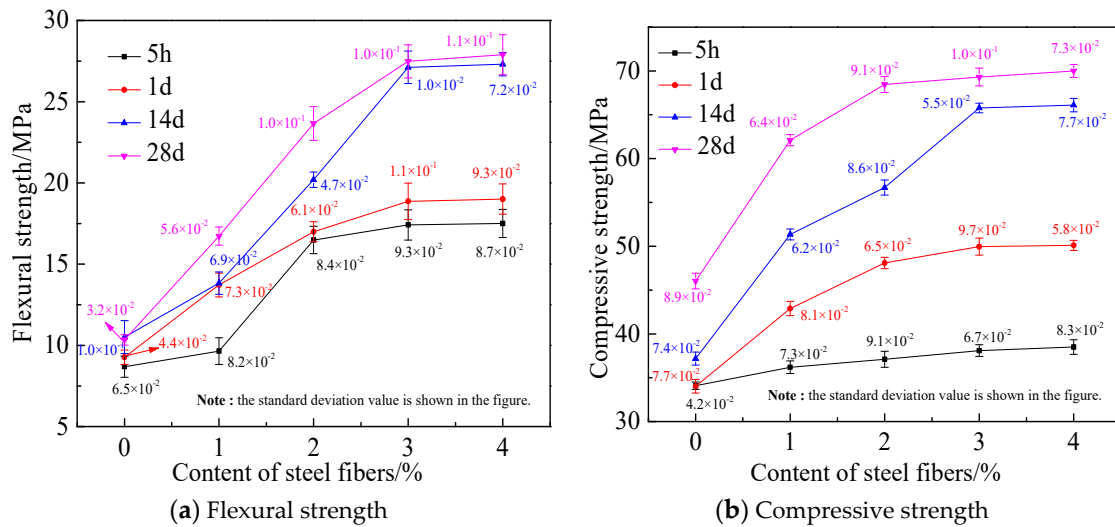


Figure 2. Mechanical strength of sulphoaluminate cement reactive powder concrete (RPC).

### 3.2. Mass Loss with Freeze–Thaw Cycles

As presented from Section 3.1, steel fibers of 3.0% was the threshold value of mechanical strength. Therefore, in the experiment of freeze–thaw cycles, specimens were prepared with 3.0% steel fibers.

Figure 3 shows the mass loss ( $\Delta m/m$ ) of sulphoaluminate cement RPC varying with the freeze–thaw cycles (N). It can be found that the mass loss of sulphoaluminate cement RPC increased linearly with the increasing freeze–thaw cycles. As indicated in previous studies [25], the freezing temperature of cement-based material was  $-2.3 \sim -2$  °C when the concentration of NaCl was 3%. Therefore, sulphoaluminate cement RPC experienced NaCl freeze–thaw cycles with the temperature ranging between  $-15$  and  $8$  °C. Consequently, some damage occurred during NaCl freeze–thaw cycles. Moreover, when the samples were immersed in NaCl solution before freeze–thaw cycles, the addition of NaCl led to increasing the absorption and water holding capacity for RPC samples, thus increasing initial water saturation [26]. Additionally, the permeable pressure and the freezing speed are increased and subsequently the surface scaling deterioration is induced [27]. Finally, as depicted in Figure 3, the mass of sulphoaluminate cement RPC with cyclic loading treatment decreased more obviously than that without cyclic loading due to the initial crack induced by cyclic loading. Figure 3 shows that the mass loss of sulphoaluminate cement RPC was less than 4%. This result indicated that sulphoaluminate cement RPC showed excellent resistance to NaCl freeze–thaw cycles.

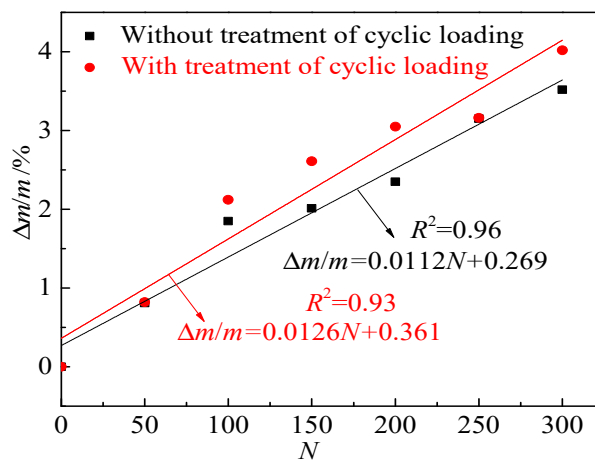


Figure 3. Mass loss during freeze–thaw cycles.

### 3.3. Variation of Mechanical Performance during Freeze-Thaw Cycles

Figures 4 and 5 show the mechanical strength (flexural and compressive strengths) loss ( $\Delta f_i/f_i$  and  $\Delta f_{cu}/f_{cu}$ ) of sulphoaluminate cement RPC during freeze–thaw cycles. It can be found that the flexural strength loss increased with an exponential function, while the compressive strength loss increased linearly with the freeze–thaw cycles due to the freeze–thaw damage [15]. The flexural and compressive strengths losses of sulphoaluminate cement RPC without cyclic loading treatment were 0~18.7% and 0~26.8%. However, when cyclic loading was applied in specimens before freeze–thaw cycles, the flexural and compressive strengths losses of sulphoaluminate RPC were 0~7.5% and 0~23.7%. It was obtained from Figures 4 and 5 that the flexural strength decayed more seriously than compressive strength during the freeze–thaw cycles. As depicted in Figures 3 and 4, cyclic loading led to more mechanical strength loss.

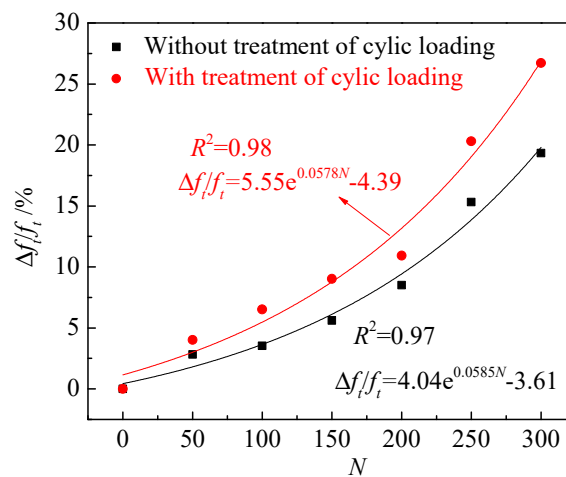


Figure 4. Flexural strength loss during freeze–thaw cycles.

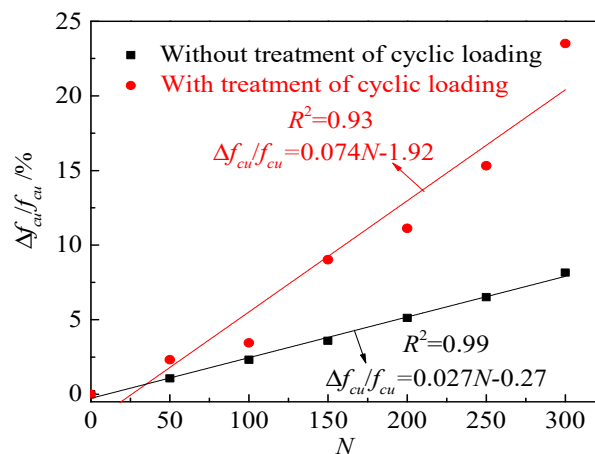


Figure 5. Compressive strength loss during freeze–thaw cycles.

Figure 6 shows the RDME values varying with the freeze–thaw cycles. As observed from Figure 6, the RDME decreased linearly with the freeze–thaw cycles due to the inner cracks, which hindered sound speed. RDME of specimens decreased more rapidly when cyclic loading was exerted on the specimens. This was attributed to the fact that some initial cracks occurred, leading to the more severe attenuation of sulphoaluminate cement RPC [28]. The RDME of specimens varied from 100% to 84.3% when the specimens were not disposed of cyclic loading before freeze–thaw cycles. Meanwhile, when the cyclic loading was exerted on specimens, the RDME of specimens varied from 100% to 74.6%.

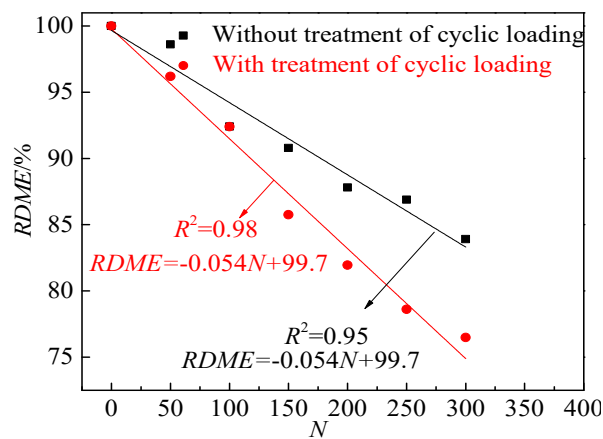


Figure 6. The RDME values during freeze–thaw cycles.

### 3.4. Chloride Migration Coefficient during Freeze–Thaw Cycles

Figure 7 shows the chloride migration coefficient during freeze–thaw cycles. As depicted in Figure 7, the chloride migration coefficient increased linearly with the increased freeze–thaw cycles. The chloride migration coefficient during freeze–thaw cycles of specimens without cyclic loading before freeze–thaw cycles was  $2.1 \times 10^{-12}/(\text{m}^2/\text{s}) \sim 7.8 \times 10^{-12}/(\text{m}^2/\text{s})$ . While, when cyclic loading was exerted on the specimens, the chloride migration coefficient during freeze–thaw cycles of specimens was  $2.8 \times 10^{-12}/(\text{m}^2/\text{s}) \sim 9.1 \times 10^{-12}/(\text{m}^2/\text{s})$ . As shown in Figure 7, the cyclic loading accelerated the freeze–thaw damage, thus increasing the chloride migration coefficient.

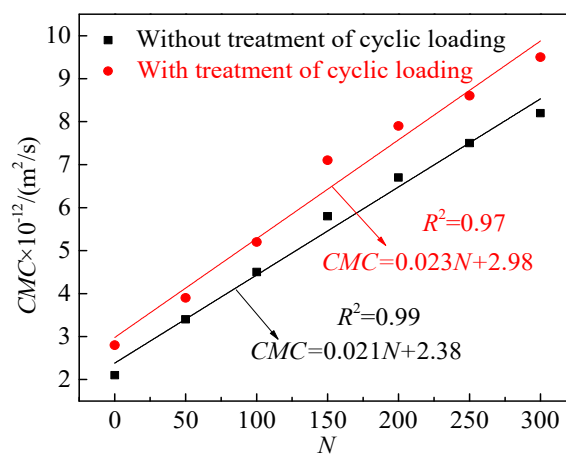


Figure 7. The chloride migration coefficient during freeze–thaw cycles.

## 4. Conclusions

In this study, the mechanical strength, the influence of NaCl freeze thaw cycles and cyclic loading on the mechanical performance and permeability of sulphoaluminate cement RPC were investigated. The main findings of this manuscript can be summarized below:

The mechanical strengths of sulphoaluminate cement RPC were improved with increasing dosage of steel fibers and the increasing curing age. In terms of mechanical strengths, the optimal percentage of steel fibers and the curing age threshold were 3.0% and 14 days, respectively. Additionally, sulphoaluminate cement RPC could reach a high level: the flexural strength (8.69~17.51 MPa) and the compressive strength (34.1~38.5 MPa) for an early curing age of 5 h.

The parameters including mass loss, the chloride migration coefficient and the compressive strength loss showed increasing linear relationship with freeze–thaw cycles, while the flexural strength

loss increased exponentially with freeze–thaw cycles and the relative dynamic modulus of elasticity decreased linearly with the increased freeze–thaw cycles.

Cyclic loading accelerated the deterioration of sulphoaluminate cement RPC's mechanical strengths and increased the chloride migration in concrete.

**Author Contributions:** Conceptualization, methodology, software and writing—original draft preparation, X.H. and H.W.; validation and supervision, F.S.; project administration, H.W.; X.H.; formal analysis, H.W. All authors have read and agreed to the published version of the manuscript.

**Funding:** This work is sponsored by the National Natural Science Foundation of China (No.51808300 and 51803185), Public Welfare Project of Zhejiang Province (LGF21E030005), China Postdoctoral Science Foundation (2020M681917), Postdoctoral Foundation of Zhejiang Sci-tech University Tongxiang Research Institute (TYY202013).

**Conflicts of Interest:** The authors declare no conflict of interest.

## References

1. Rajasekar, A.; Arunachalam, K.; Kottaisamy, M. Durability of ultra-high strength concrete with waste granite sand as partial substitute for aggregate. *J. Comput. Theor. Nanosci.* **2018**, *15*, 446–452. [[CrossRef](#)]
2. Dong, S.; Dong, X.; Ashour, A.; Han, B.; Ou, J. Fracture and self-sensing characteristics of super-fine stainless wire reinforced reactive powder concrete. *Cem. Concr. Compos.* **2020**, *105*, 103427. [[CrossRef](#)]
3. Wen, S.; Chung, D.D.L. A comparative study of steel-and carbon-fibre cement as piezoresistive strain sensors. *Adv. Cem. Res.* **2003**, *15*, 119–128. [[CrossRef](#)]
4. Xu, L.; Liu, S.; Li, N.; Peng, Y.; Wu, K.; Wang, P. Retardation effect of elevated temperature on the setting of calcium sulfoaluminate cement clinker. *Constr. Build. Mater.* **2018**, *178*, 112–119. [[CrossRef](#)]
5. Wang, H.; Gao, X.; Liu, J.; Ren, M.; Lu, A. Multi-functional properties of carbon nanofiber reinforced reactive powder concrete. *Constr. Build. Mater.* **2018**, *187*, 699–707. [[CrossRef](#)]
6. Dong, S.; Han, B.; Ou, J.; Li, Z.; Han, L.; Yu, X. Electrically conductive behaviors and mechanisms of short-cut super-fine stainless wire reinforced reactive powder concrete. *Cem. Concr. Compos.* **2016**, *72*, 48–65. [[CrossRef](#)]
7. Huang, H.; Gao, X.; Li, L.; Wang, H. Improvement effect of steel fiber orientation control on mechanical performance of UHPC. *Constr. Build. Mater.* **2018**, *188*, 709–721. [[CrossRef](#)]
8. Nematollahzade, M.; Tajadini, A.; Afshoon, I.; Aslani, F. Influence of different curing conditions and water to cement ratio on properties of self-compacting concretes. *Constr. Build. Mater.* **2020**, *237*, 117570. [[CrossRef](#)]
9. Feng, H.; Chen, G.; Hadi, M.N.; Sheikh, M.N.; Zhou, B. Mechanical behaviour of micro-fine steel fibre reinforced sulphoaluminate cement composite. *Constr. Build. Mater.* **2018**, *170*, 91–100. [[CrossRef](#)]
10. Mohd, S.; Jagdish, P.; Amjad, M. Effect of GGBFS on time dependent compressive strength of concrete. *Constr. Build. Mater.* **2010**, *24*, 1469–1478.
11. Sajedi, F.; Razak, H. Effects of curing regimes and cement fineness on the compressive strength of ordinary Portland cement mortars. *Constr. Build. Mater.* **2011**, *25*, 2036–2045. [[CrossRef](#)]
12. Singh, M.; Kapur, P.C.; Pradip, P. Preparation of calcium sulphoaluminate cement using fertiliser plant wastes. *J. Hazard. Mater.* **2008**, *157*, 106–113. [[CrossRef](#)] [[PubMed](#)]
13. Chen, P.; Ma, B.; Tan, H.; Liu, X.; Zhang, T.; Li, C.; Yang, Q.; Luo, Z. Utilization of barium slag to improve chloride-binding ability of cement-based material. *J. Clean. Prod.* **2020**, 124612. [[CrossRef](#)]
14. Liu, Q.F.; Iqbal, M.F.; Yang, J.; Lu, X.Y.; Zhang, P.; Rauf, M. Prediction of chloride diffusivity in concrete using artificial neural network: Modelling and performance evaluation. *Constr. Build. Mater.* **2020**, *266*, 12108.
15. Mao, L.X.; Hu, Z.; Xia, J.; Feng, G.L.; Azim, I.; Yang, J.; Liu, Q.F. Multi-phase modelling of electrochemical rehabilitation for ASR and chloride affected concrete composites. *Compos. Struct.* **2019**, *207*, 176–189. [[CrossRef](#)]
16. Liu, Q.F.; Feng, G.L.; Xia, J.; Yang, J.; Li, L.Y. Ionic transport features in concrete composites containing various shaped aggregates: A numerical study. *Compos. Struct.* **2018**, *183*, 371–380. [[CrossRef](#)]
17. Wang, H.; Zhang, A.; Zhang, L.; Liu, J.; Han, Y.; Shu, H.; Wang, J. Study on the influence of compound rust inhibitor on corrosion of steel bars in chloride concrete by electrical parameters. *Constr. Build. Mater.* **2020**, *262*, 120763. [[CrossRef](#)]
18. GB175-2007. *Common Portland Cement*; China Standard Press: Beijing, China, 2007. (In Chinese)
19. GB/T21236-2007. *Silica Fume from Electric-Furnace*; China Standard Press: Beijing, China, 2007. (In Chinese)

20. GB/T18046-2008. *Ground Granulated Blast Furnace Slag Used for Cement and Concrete*; China Standard Press: Beijing, China, 2007. (In Chinese)
21. GB/T17671-1999. *Method of Testing Cements-Determination of Strength*; China Standard Press: Beijing, China, 1999. (In Chinese)
22. GB/T 50082-2009. *Standard for Test Method of Long-Term Performance and Durability of Ordinary Concrete*; China Standard Press: Beijing, China, 2009. (In Chinese)
23. Ma, B.; Li, H.; Mei, J.; Li, X. Influence of nano-SiO<sub>2</sub> addition on properties of sulphoaluminate cement based material. *J. Wuhan Univ. Technol.-Mater. Sci. Ed.* **2017**, *32*, 106–112. [[CrossRef](#)]
24. Cai, G.; Zhao, J. Application of sulphoaluminate cement to repair deteriorated concrete members in chloride ion rich environment-A basic experimental investigation of durability properties. *KSCE J. Civ. Eng.* **2016**, *20*, 2832–2841. [[CrossRef](#)]
25. Shi, X.; Fay, L.; Peterson, M.; Yang, Z. Freeze-thaw damage and chemical change of a portland cement concrete in the presence of diluted deicers. *Mater. Struct.* **2010**, *43*, 933–946. [[CrossRef](#)]
26. Ding, Y.; Huang, Y.; Zhang, Y.; Jalali, S.; Aguiar, J.B. Self-monitoring of freeze-thaw damage using triphasic electric conductive concrete. *Constr. Build. Mater.* **2015**, *101*, 440–446. [[CrossRef](#)]
27. Wang, Z.; Zeng, Q.; Wang, L.; Yao, Y.; Li, K. Characterizing blended cement pastes under cyclic freeze-thaw actions by electrical resistivity. *Constr. Build. Mater.* **2013**, *44*, 477–486. [[CrossRef](#)]
28. Wang, H.; Gao, X.; Liu, J. Effects of salt freeze-thaw cycles and cyclic loading on the piezoresistive properties of carbon nanofibers mortar. *Constr. Build. Mater.* **2018**, *177*, 192–201. [[CrossRef](#)]

**Publisher’s Note:** MDPI stays neutral with regard to jurisdictional claims in published maps and institutional affiliations.



© 2020 by the authors. Licensee MDPI, Basel, Switzerland. This article is an open access article distributed under the terms and conditions of the Creative Commons Attribution (CC BY) license (<http://creativecommons.org/licenses/by/4.0/>).